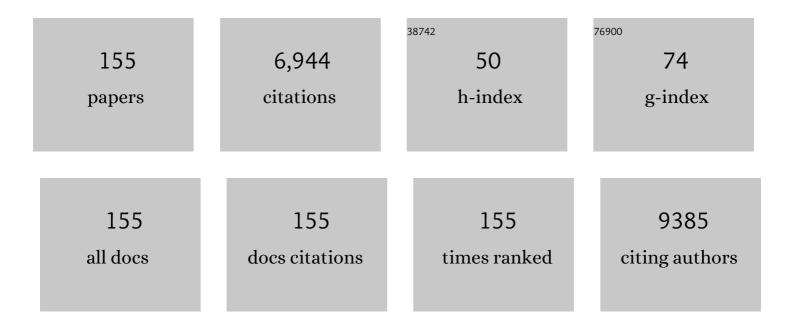
List of Publications by Year in descending order

Source: https://exaly.com/author-pdf/12143973/publications.pdf Version: 2024-02-01



УИСНЕМС М/И

#	Article	IF	CITATIONS
1	Microstructure and compression properties of a dual-phase FeCoCrMn high-entropy alloy. Advanced Composites and Hybrid Materials, 2022, 5, 1508-1515.	21.1	10
2	Highly efficient solar-driven photocatalytic hydrogen evolution with FeMoSx/mpg-C3N4 heterostructure. Chemical Engineering Journal, 2022, 427, 131507.	12.7	4
3	Synergy between fungi and bacteria promotes polycyclic aromatic hydrocarbon cometabolism in lignin-amended soil. Journal of Hazardous Materials, 2022, 425, 127958.	12.4	21
4	Al doped Ni-Co layered double hydroxides with surface-sulphuration for highly stable flexible supercapacitors. Journal of Colloid and Interface Science, 2022, 615, 173-183.	9.4	19
5	Layer-by-Layer Assembly of CeO _{2–<i>x</i>} @C-rGO Nanocomposites and CNTs as a Multifunctional Separator Coating for Highly Stable Lithium–Sulfur Batteries. ACS Applied Materials & Interfaces, 2022, 14, 18634-18645.	8.0	24
6	Moisture effects on the active prokaryotic communities in a saline soil unraveled by 180-informed metagenomics. Journal of Soils and Sediments, 2021, 21, 430-440.	3.0	6
7	Self-Locomotive Soft Actuator Based on Asymmetric Microstructural Ti ₃ C ₂ T _{<i>x</i>} MXene Film Driven by Natural Sunlight Fluctuation. ACS Nano, 2021, 15, 5294-5306.	14.6	103
8	Carbon Nanolayer-Wrapped Mesoporous TiO ₂ –B/Anatase for Li ⁺ Storage. ACS Applied Nano Materials, 2021, 4, 7832-7839.	5.0	8
9	Lightâ€Driven Selfâ€Oscillating Actuators with Phototactic Locomotion Based on Black Phosphorus Heterostructure. Angewandte Chemie, 2021, 133, 20674-20680.	2.0	3
10	Lightâ€Driven Selfâ€Oscillating Actuators with Phototactic Locomotion Based on Black Phosphorus Heterostructure. Angewandte Chemie - International Edition, 2021, 60, 20511-20517.	13.8	82
11	Zinc doped Fe2O3 hierarchical particles for stable all-solid-state Ni-Co/Fe battery. Journal of Alloys and Compounds, 2021, 879, 160436.	5.5	4
12	Designing core–shell metal–organic framework hybrids: toward high-efficiency electrochemical potassium storage. Journal of Materials Chemistry A, 2021, 9, 26181-26188.	10.3	10
13	Progress of low-frequency sound absorption research utilizing intelligent materials and acoustic metamaterials. RSC Advances, 2021, 11, 37784-37800.	3.6	20
14	Zn–Co Sulfide Microflowers Anchored on Threeâ€Dimensional Graphene: A Highâ€Capacitance and Longâ€Cycleâ€Life Electrode for Asymmetric Supercapacitors. Chemistry - A European Journal, 2020, 26, 650-658.	3.3	21
15	Influence of organic amendments used for benz[a]anthracene remediation in a farmland soil: pollutant distribution and bacterial changes. Journal of Soils and Sediments, 2020, 20, 32-41.	3.0	11
16	Rational Design of Nanostructured Electrode Materials toward Multifunctional Supercapacitors. Advanced Functional Materials, 2020, 30, 1902564.	14.9	252
17	Synthesis of Niâ^'MoS _x /g ₃ N ₄ for Photocatalytic Hydrogen Evolution under Visible Light. ChemCatChem, 2020, 12, 911-916.	3.7	18
18	A surface precleaning strategy intensifies the interface coupling of the Bi ₂ O ₃ /TiO ₂ heterostructure for enhanced photoelectrochemical detection properties. Materials Chemistry Frontiers, 2020, 4, 638-644.	5.9	9

#	Article	IF	CITATIONS
19	CoO Quantum Dots Anchored on Reduced Graphene Oxide Aerogels for Lithium-Ion Storage. ACS Applied Nano Materials, 2020, 3, 10369-10379.	5.0	16
20	Synthesis of SrTiO ₃ submicron cubes with simultaneous and competitive photocatalytic activity for H ₂ O splitting and CO ₂ reduction. RSC Advances, 2020, 10, 42619-42627.	3.6	10
21	Rational Regulation of Surface Free Radicals on TiO2 Nanotube Arrays via Ag2O–AgBiO3 towards Enhanced Selective Photoelectrochemical Detection. Nanomaterials, 2020, 10, 2002.	4.1	1
22	Directly Exfoliated Ultrathin Silicon Nanosheets for Enhanced Photocatalytic Hydrogen Production. Journal of Physical Chemistry Letters, 2020, 11, 8668-8674.	4.6	14
23	Enhanced Energy Storage Performance of 3D Hybrid Metal Sulfides via Synergistic Engineering of Architecture and Composition. ACS Sustainable Chemistry and Engineering, 2020, 8, 11491-11500.	6.7	5
24	Assembling of Bi atoms on TiO ₂ nanorods boosts photoelectrochemical water splitting of semiconductors. Nanoscale, 2020, 12, 4302-4308.	5.6	49
25	Ni–Co coordination hollow spheres for high performance flexible all-solid-state supercapacitor. Electrochimica Acta, 2020, 337, 135828.	5.2	27
26	An Autonomous Soft Actuator with Lightâ€Driven Selfâ€Sustained Wavelike Oscillation for Phototactic Selfâ€Locomotion and Power Generation. Advanced Functional Materials, 2020, 30, 1908842.	14.9	100
27	MoS2 quantum dots decorated ultrathin NiO nanosheets for overall water splitting. Journal of Colloid and Interface Science, 2020, 566, 411-418.	9.4	38
28	In situ electrochemical oxidation of electrodeposited Ni-based nanostructure promotes alkaline hydrogen production. Nanotechnology, 2019, 30, 474001.	2.6	5
29	Enhanced Visible-Light Photocatalytic Remediation of Tetracycline Hydrochloride by Nanostructured BiOI Homojunctions. Nano, 2019, 14, 1950112.	1.0	6
30	Grapheneâ€Based Bimorph Actuators with Dualâ€Response and Largeâ€Deformation by a Simple Method. Macromolecular Materials and Engineering, 2019, 304, 1800688.	3.6	22
31	Multifunctional Soft Actuators Based on Anisotropic Paper/Polymer Bilayer Toward Bioinspired Applications. Advanced Materials Technologies, 2019, 4, 1800674.	5.8	37
32	Coordination derived stable Ni–Co MOFs for foldable all-solid-state supercapacitors with high specific energy. Journal of Materials Chemistry A, 2019, 7, 4998-5008.	10.3	133
33	A bioinspired multi-functional wearable sensor with an integrated light-induced actuator based on an asymmetric graphene composite film. Journal of Materials Chemistry C, 2019, 7, 6879-6888.	5.5	42
34	Water-Soluble Defect-Rich MoS ₂ Ultrathin Nanosheets for Enhanced Hydrogen Evolution. Journal of Physical Chemistry Letters, 2019, 10, 3282-3289.	4.6	50
35	Systematic study on hybrid supercapacitor of Ni-Co layered double hydroxide//activated carbons. Electrochimica Acta, 2019, 305, 403-415.	5.2	58
36	Z-scheme carbon-bridged Bi2O3/TiO2 nanotube arrays to boost photoelectrochemical detection performance. Applied Catalysis B: Environmental, 2019, 248, 255-263.	20.2	85

#	Article	IF	CITATIONS
37	Carbonâ€Bridged g ₃ N ₄ Nanosheets for High Hydrogen Evolution Rate by a Two‧tep Gaseous Treatment. ChemistrySelect, 2019, 4, 13064-13070.	1.5	6
38	SBA-15 Templated Mesoporous Graphitic C ₃ N ₄ for Remarkably Enhanced Photocatalytic Degradation of Organic Pollutants under Visible Light. Nano, 2019, 14, 1950136.	1.0	8
39	High rate capability electrode constructed by anchoring CuCo2S4 on graphene aerogel skeleton toward quasi-solid-state supercapacitor. Electrochimica Acta, 2019, 298, 321-329.	5.2	68
40	Enhanced High-Temperature Cyclic Stability of Al-Doped Manganese Dioxide and Morphology Evolution Study Through in situ NMR under High Magnetic Field. ACS Applied Materials & Interfaces, 2018, 10, 9398-9406.	8.0	36
41	Contributions of ryegrass, lignin and rhamnolipid to polycyclic aromatic hydrocarbon dissipation in an arable soil. Soil Biology and Biochemistry, 2018, 118, 27-34.	8.8	39
42	Porous HKUST-1 derived CuO/Cu2O shell wrapped Cu(OH)2 derived CuO/Cu2O core nanowire arrays for electrochemical nonenzymatic glucose sensors with ultrahigh sensitivity. Applied Surface Science, 2018, 439, 11-17.	6.1	69
43	Oxygenated derivative is more influential than unsubstituted polycyclic aromatic hydrocarbon on ammonia-oxidizing archaea in an acidic soil. Journal of Soils and Sediments, 2018, 18, 2573-2580.	3.0	4
44	Ni(OH) ₂ /CNTs hierarchical spheres for a foldable all-solid-state supercapacitor with high specific energy. Nanoscale, 2018, 10, 7377-7381.	5.6	52
45	Supercapacitive performance of single phase CuO nanosheet arrays with ultra-long cycling stability. Journal of Alloys and Compounds, 2018, 753, 731-739.	5.5	10
46	MOF-74 derived porous hybrid metal oxide hollow nanowires for high-performance electrochemical energy storage. Journal of Materials Chemistry A, 2018, 6, 8396-8404.	10.3	101
47	Interface design in 3D-SiC/Al-Si-Mg interpenetrating composite fabricated by pressureless infiltration. Ceramics International, 2018, 44, 11956-11965.	4.8	25
48	Microstructures and Properties of 40Cu/Ag(Invar) Composites Fabricated by Powder Metallurgy and Subsequent Thermo-Mechanical Treatment. Metallurgical and Materials Transactions A: Physical Metallurgy and Materials Science, 2018, 49, 1869-1878.	2.2	6
49	g-C ₃ N ₄ /g-C ₃ N ₄ isotype heterojunction as an efficient platform for direct photodegradation of antibiotic. Fullerenes Nanotubes and Carbon Nanostructures, 2018, 26, 210-217.	2.1	32
50	NiS and MoS2 nanosheet co-modified graphitic C3N4 ternary heterostructure for high efficient visible light photodegradation of antibiotic. Journal of Hazardous Materials, 2018, 341, 10-19.	12.4	179
51	Fabrication, microstructures and properties of 50â€vol% SiCp/6061Al composites via a pressureless sintering technique. Powder Metallurgy, 2018, 61, 1-9.	1.7	12
52	Precipitation and its strengthening of Cu-rich phase in CrMnFeCoNiCux high-entropy alloys. Materials Science & Engineering A: Structural Materials: Properties, Microstructure and Processing, 2018, 713, 134-140.	5.6	99
53	CeO _{2â^'x} /C/rGO nanocomposites derived from Ce-MOF and graphene oxide as a robust platform for highly sensitive uric acid detection. Nanoscale, 2018, 10, 1939-1945.	5.6	88
54	Self-recovery in Li-metal hybrid lithium-ion batteries <i>via</i> WO ₃ reduction. Nanoscale, 2018, 10, 15956-15966.	5.6	87

#	Article	IF	CITATIONS
55	3D Coral-Like Ni ₃ S ₂ on Ni Foam as a Bifunctional Electrocatalyst for Overall Water Splitting. ACS Applied Materials & Interfaces, 2018, 10, 31330-31339.	8.0	80
56	Multimodal particle distribution in 3D-SiC/Al-Si-Mg interpenetrating composite fabricated by pressureless infiltration. Ceramics International, 2018, 44, 19851-19858.	4.8	22
57	Self-healing polyaniline-graphene oxides based electrodes with enhanced cycling stability. Electrochimica Acta, 2018, 282, 835-844.	5.2	25
58	Synthesis and supercapacitive performance of CuO/Cu2O nanosheet arrays modified by hydrothermal deposited NiOOH. Journal of Solid State Electrochemistry, 2017, 21, 1489-1497.	2.5	14
59	In-situ constructing NiO nanoplatelets network on La 0.75 Sr 0.25 Mn 0.5 Cr 0.5 O 3-δ electrode with enhanced steam electrolysis. International Journal of Hydrogen Energy, 2017, 42, 5657-5666.	7.1	4
60	A high-entropy V 35 Ti 35 Fe 15 Cr 10 Zr 5 alloy with excellent high-temperature strength. Materials and Design, 2017, 121, 229-236.	7.0	61
61	The anodization synthesis of copper oxide nanosheet arrays and their photoelectrochemical properties. Applied Surface Science, 2017, 412, 505-516.	6.1	41
62	pH is the primary determinant of the bacterial community structure in agricultural soils impacted by polycyclic aromatic hydrocarbon pollution. Scientific Reports, 2017, 7, 40093.	3.3	144
63	Synthesis of W2N nanorods-graphene hybrid structure with enhanced oxygen reduction reaction performance. International Journal of Hydrogen Energy, 2017, 42, 25924-25932.	7.1	14
64	Electrically and Sunlightâ€Driven Actuator with Versatile Biomimetic Motions Based on Rolled Carbon Nanotube Bilayer Composite. Advanced Functional Materials, 2017, 27, 1704388.	14.9	211
65	Construction of NiO/MnO2/CeO2 hybrid nanoflake arrays as platform for electrochemical energy storage. Journal of Power Sources, 2017, 361, 310-317.	7.8	35
66	Cryo-mediated exfoliation and fracturing of layered materials into 2D quantum dots. Science Advances, 2017, 3, e1701500.	10.3	91
67	Flexible Supercapacitors Based on Solid Ion Conducting Polymer with High Mechanical Strength. Journal of the Electrochemical Society, 2017, 164, A1952-A1957.	2.9	34
68	Enhanced thermal conductive 3D-SiC/Al-Si-Mg interpenetrating composites fabricated by pressureless infiltration. Ceramics International, 2017, 43, 1755-1761.	4.8	59
69	Supercapacitive performance of homogeneous Co3O4/TiO2 nanotube arrays enhanced by carbon layer and oxygen vacancies. Journal of Solid State Electrochemistry, 2017, 21, 1069-1078.	2.5	17
70	One-step electrodeposition of Co 0·12 Ni 1·88 S 2 @Co 8 S 9 nanoparticles on highly conductive TiO 2 nanotube arrays for battery-type electrodes with enhanced energy storage performance. Journal of Power Sources, 2017, 364, 400-409.	7.8	17
71	Photoelectrochemical detection performance and mechanism discussion of Bi ₂ O ₃ modified TiO ₂ nanotube arrays. RSC Advances, 2016, 6, 61367-61377.	3.6	14
72	In-situ constructing hybrid oxygen electrode of porous Co3O4 nanowire array on La0.8Sr0.2MnO3â^'δ for steam electrolysis. International Journal of Hydrogen Energy, 2016, 41, 5428-5436.	7.1	6

#	Article	IF	CITATIONS
73	Supercapacitive performance of electrochemically doped TiO ₂ nanotube arrays decorated with Cu ₂ 0 nanoparticles. RSC Advances, 2016, 6, 47669-47675.	3.6	14
74	Controllable synthesis of graphitic C ₃ N ₄ /ultrathin MoS ₂ nanosheet hybrid nanostructures with enhanced photocatalytic performance. Dalton Transactions, 2016, 45, 15406-15414.	3.3	104
75	Construction of CuO/Cu2O@CoO core shell nanowire arrays for high-performance supercapacitors. Surface and Coatings Technology, 2016, 299, 15-21.	4.8	49
76	Fabrication and photocatalytic performances of BiOCl nanosheets modified with ultrafine Bi ₂ O ₃ nanocrystals. RSC Advances, 2016, 6, 63241-63249.	3.6	11
77	Integration of mesoporous nickel cobalt oxide nanosheets with ultrathin layer carbon wrapped TiO ₂ nanotube arrays for high-performance supercapacitors. New Journal of Chemistry, 2016, 40, 6881-6889.	2.8	18
78	Long Cyclic Life in Manganese Oxide-Based Electrodes. ACS Applied Materials & Interfaces, 2016, 8, 18078-18088.	8.0	35
79	Oxidation of polycyclic aromatic hydrocarbons using Bacillus subtilis CotA with high laccase activity and copper independence. Chemosphere, 2016, 148, 1-7.	8.2	74
80	Hydrothermal synthesis of layered molybdenum sulfide/N-doped graphene hybrid with enhanced supercapacitor performance. Carbon, 2016, 99, 35-42.	10.3	183
81	Synthesis and adsorption properties of halloysite/carbon nanocomposites and halloysite-derived carbon nanotubes. Applied Clay Science, 2016, 119, 284-293.	5.2	53
82	Effects of pH and polycyclic aromatic hydrocarbon pollution on thaumarchaeotal community in agricultural soils. Journal of Soils and Sediments, 2016, 16, 1960-1969.	3.0	16
83	All solid supercapacitors based on an anion conducting polymer electrolyte. RSC Advances, 2016, 6, 19826-19832.	3.6	17
84	Synthesis of porous NiO/CeO ₂ hybrid nanoflake arrays as a platform for electrochemical biosensing. Nanoscale, 2016, 8, 770-774.	5.6	41
85	A chromium oxide coated nickel/yttria stabilized zirconia electrode with a heterojunction interface for use in electrochemical methane reforming. RSC Advances, 2015, 5, 47599-47608.	3.6	14
86	Controlled deposition and enhanced visible light photocatalytic performance of Pt-modified TiO2 nanotube arrays. Applied Surface Science, 2015, 351, 225-231.	6.1	53
87	Electrochemical Biosensor based on Pt/Au Alloy Nanowire Arrays for Phosphate Detection. Journal of the Electrochemical Society, 2015, 162, B62-B67.	2.9	34
88	Composite manganate oxygen electrode enhanced with iron oxide nanocatalyst for high temperature steam electrolysis in a proton-conducting solid oxide electrolyzer. International Journal of Hydrogen Energy, 2015, 40, 7920-7931.	7.1	26
89	Profiling bacterial diversity in a limestone cave of the western Loess Plateau of China. Frontiers in Microbiology, 2015, 6, 244.	3.5	80
90	Photocatalytic property of a Bi ₂ O ₃ nanoparticle modified BiOCl composite with a nanolayered hierarchical structure synthesized by in situ reactions. Dalton Transactions, 2015, 44, 5386-5395.	3.3	38

#	Article	IF	CITATIONS
91	Activated carbon coated palygorskite as adsorbent by activation and its adsorption for methylene blue. Journal of Environmental Sciences, 2015, 33, 97-105.	6.1	56
92	A facile synthesis of mesoporous Co ₃ O ₄ /CeO ₂ hybrid nanowire arrays for high performance supercapacitors. Journal of Materials Chemistry A, 2015, 3, 10425-10431.	10.3	108
93	Structural Evolution and Property of Hot-pressed Palygorskite Clay. Transactions of the Indian Ceramic Society, 2015, 74, 169-176.	1.0	2
94	Efficient Carbon Dioxide Electrolysis Based on Perovskite Cathode Enhanced with Nickel Nanocatalyst. Electrochimica Acta, 2015, 153, 325-333.	5.2	44
95	A composite cathode based on scandium-doped chromate for direct high-temperature steam electrolysis in a symmetric solid oxide electrolyzer. Journal of Power Sources, 2015, 274, 718-729.	7.8	51
96	Chromate cathode decorated with in-situ growth of copper nanocatalyst for high temperature carbon dioxide electrolysis. International Journal of Hydrogen Energy, 2014, 39, 20888-20897.	7.1	54
97	A Flow-Injection Photoelectrochemical Sensor Based on TiO ₂ Nanotube Arrays for Organic Compound Detection. Journal of the Electrochemical Society, 2014, 161, H57-H61.	2.9	17
98	Perovskite chromates cathode with resolved and anchored nickel nano-particles for direct high-temperature steam electrolysis. Journal of Power Sources, 2014, 246, 346-355.	7.8	30
99	Composite cathode La0.4Sr0.4TiO3â^'δ–Ce0.8Sm0.2O2â^'δ impregnated with Ni for high-temperature steam electrolysis. Journal of Power Sources, 2014, 245, 245-255.	7.8	46
100	Integration of a highly ordered gold nanowires array with glucose oxidase for ultra-sensitive glucose detection. Analytica Chimica Acta, 2014, 809, 134-140.	5.4	37
101	Ultrasensitive detection of mercury with a novel one-step signal amplified lateral flow strip based on gold nanoparticle-labeled ssDNA recognition and enhancement probes. Biosensors and Bioelectronics, 2014, 61, 14-20.	10.1	65
102	Reversibly in-situ anchoring copper nanocatalyst inÂperovskite titanate cathode for direct high-temperature steam electrolysis. International Journal of Hydrogen Energy, 2014, 39, 5485-5496.	7.1	48
103	Composite cathode based on doped vanadate enhanced with loaded metal nanoparticles for steam electrolysis. Journal of Power Sources, 2014, 253, 349-359.	7.8	20
104	Synthesis of clay/carbon adsorbent through hydrothermal carbonization of cellulose on palygorskite. Applied Clay Science, 2014, 95, 60-66.	5.2	58
105	Ammonia oxidation-dependent growth of group I.1b <i>Thaumarchaeota</i> in acidic red soil microcosms. FEMS Microbiology Ecology, 2014, 89, 127-134.	2.7	17
106	Composite titanate cathode decorated with heterogeneous electrocatalytic sites towards efficient carbon dioxide electrolysis. RSC Advances, 2014, 4, 22697-22709.	3.6	22
107	Demonstration of efficient electrochemical biogas reforming in a solid oxide electrolyser with titanate cathode. RSC Advances, 2014, 4, 38474-38483.	3.6	11
108	Remarkable chemical adsorption of manganese-doped titanate for direct carbon dioxide electrolysis. Journal of Materials Chemistry A, 2014, 2, 6904-6915.	10.3	137

#	Article	IF	CITATIONS
109	Redox-reversible niobium-doped strontium titanate decorated with in situ grown nickel nanocatalyst for high-temperature direct steam electrolysis. Dalton Transactions, 2014, 43, 14147.	3.3	33
110	A composite cathode based on scandium doped titanate with enhanced electrocatalytic activity towards direct carbon dioxide electrolysis. Physical Chemistry Chemical Physics, 2014, 16, 21417-21428.	2.8	37
111	Single-phase nickel-doped ceria cathode with in situ grown nickel nanocatalyst for direct high-temperature carbon dioxide electrolysis. RSC Advances, 2014, 4, 40494-40504.	3.6	26
112	Photocatalytic properties of Bi/BiOCl heterojunctions synthesized using an in situ reduction method. New Journal of Chemistry, 2014, 38, 4913-4921.	2.8	74
113	Enhanced visible-light photoelectrochemical behaviour of heterojunction composite with Cu ₂ 0 nanoparticles-decorated TiO ₂ nanotube arrays. New Journal of Chemistry, 2014, 38, 4975-4984.	2.8	47
114	Perovskite titanate cathode decorated by grown iron nanocatalyst with enhanced electrocatalytic activity for high-temperature steam electrolysis. Electrochimica Acta, 2014, 127, 215-227.	5.2	34
115	Photoelectrochemical properties of TiO2 Nanotube Arrays Modified with BiOCl nanosheets. Electrochimica Acta, 2014, 130, 213-221.	5.2	28
116	Photoelectrochemical Performances and Potential Applications of TiO2 Nanotube Arrays Modified with Ag and Pt Nanoparticles. Electrochimica Acta, 2014, 121, 194-202.	5.2	41
117	Quantitative SERS detection of low-concentration aromatic polychlorinated biphenyl-77 and 2,4,6-trinitrotoluene. Journal of Hazardous Materials, 2014, 280, 706-712.	12.4	44
118	Enhanced visible light photocatalytic activity of TiO2 nanotube arrays modified with CdSe nanoparticles by electrodeposition method. Surface and Coatings Technology, 2014, 242, 20-28.	4.8	20
119	In situ SERS monitoring of photocatalytic organic decomposition using recyclable TiO2-coated Ag nanowire arrays. Applied Surface Science, 2014, 301, 351-357.	6.1	49
120	Efficient carbon dioxide electrolysis in a symmetric solid oxide electrolyzer based on nanocatalyst-loaded chromate electrodes. International Journal of Hydrogen Energy, 2014, 39, 10338-10348.	7.1	35
121	In situ Growth of NixCu1-x Alloy Nanocatalysts on Redox-reversible Rutile (Nb,Ti)O4 Towards High-Temperature Carbon Dioxide Electrolysis. Scientific Reports, 2014, 4, 5156.	3.3	44
122	N, S co-doped-TiO2/fly ash beads composite material and visible light photocatalytic activity. Applied Surface Science, 2013, 284, 229-234.	6.1	73
123	Nitrogen doped TiO2 nanotube arrays with high photoelectrochemical activity for photocatalytic applications. Applied Surface Science, 2013, 280, 523-529.	6.1	82
124	One-step signal amplified lateral flow strip biosensor for ultrasensitive and on-site detection of bisphenol A (BPA) in aqueous samples. Biosensors and Bioelectronics, 2013, 49, 457-461.	10.1	92
125	Maximizing surface-enhanced Raman scattering sensitivity of surfactant-free Ag-Fe3O4 nanocomposites through optimization of silver nanoparticle density and magnetic self-assembly. Journal of Applied Physics, 2013, 114, .	2.5	37
126	Flow-through TiO2 nanotube arrays: a modified support with homogeneous distribution of Ag nanoparticles and their photocatalytic activities. New Journal of Chemistry, 2013, 37, 752.	2.8	19

#	Article	IF	CITATIONS
127	High-performance fuel electrodes based on NbTi0.5M0.5O4 (M = Ni, Cu) with reversible exsolution of the nano-catalyst for steam electrolysis. Journal of Materials Chemistry A, 2013, 1, 8984.	10.3	54
128	Composite cathode based on Ni-loaded La0.75Sr0.25Cr0.5Mn0.5O3â^î for direct steam electrolysis in an oxide-ion-conducting solid oxide electrolyzer. International Journal of Hydrogen Energy, 2013, 38, 10196-10207.	7.1	44
129	Electrochemical conversion of H2O/CO2 to fuel in a proton-conducting solid oxide electrolyser. Journal of Power Sources, 2013, 232, 187-192.	7.8	45
130	Composite cathode based on Fe-loaded LSCM for steam electrolysis in an oxide-ion-conducting solid oxide electrolyser. Journal of Power Sources, 2013, 239, 332-340.	7.8	53
131	Autotrophic Growth of Bacterial and Archaeal Ammonia Oxidizers in Freshwater Sediment Microcosms Incubated at Different Temperatures. Applied and Environmental Microbiology, 2013, 79, 3076-3084.	3.1	73
132	Perovskite Chromates Cathode with Exsolved Iron Nanoparticles for Direct High-Temperature Steam Electrolysis. ACS Applied Materials & amp; Interfaces, 2013, 5, 8553-8562.	8.0	49
133	Composite anode La _{0.8} Sr _{0.2} MnO ₃ impregnated with cobalt oxide for steam electrolysis. Proceedings of SPIE, 2013, , .	0.8	3
134	Uniformly Dispersed and Controllable Ligandâ€Free Silverâ€Nanoparticleâ€Decorated TiO ₂ Nanotube Arrays with Enhanced Photoelectrochemical Behaviors. Chemistry - an Asian Journal, 2013, 8, 2746-2754.	3.3	15
135	PREPARATION OF ULTRAFINE W – Cu COMPOSITE POWDER USING ULTRASONIC-ASSISTED ELECTROLESS PLATING. Modern Physics Letters B, 2013, 27, 1341004.	1.9	1
136	Inhibition of Bacterial Ammonia Oxidation by Organohydrazines in Soil Microcosms. Frontiers in Microbiology, 2012, 3, 10.	3.5	17
137	Molecular Detection of Novel Anammox Bacterial Clusters in the Sediments of the Shallow Freshwater Lake Taihu. Geomicrobiology Journal, 2012, 29, 852-859.	2.0	19
138	Clean and reproducible SERS substrates for high sensitive detection by solid phase synthesis and fabrication of Agâ€coated Fe ₃ O ₄ microspheres. Journal of Raman Spectroscopy, 2012, 43, 848-856.	2.5	65
139	Effect of electroless plating Ni–Cu–P layer on the wettability between cemented carbides and soldering tins. International Journal of Refractory Metals and Hard Materials, 2012, 31, 192-195.	3.8	8
140	Dissipation of polycyclic aromatic hydrocarbons (PAHs) in soil microcosms amended with mushroom cultivation substrate. Soil Biology and Biochemistry, 2012, 47, 191-197.	8.8	59
141	Nitrification activity and putative ammonia-oxidizing archaea in acidic red soils. Journal of Soils and Sediments, 2012, 12, 420-428.	3.0	36
142	A facile route to accelerate the formation of TiO2nanotube arrays. Journal of Physics: Conference Series, 2011, 276, 012047.	0.4	1
143	Rapid anodic oxidation of highly ordered TiO2 nanotube arrays. Journal of Alloys and Compounds, 2011, 509, L157-L160.	5.5	42
144	Preparation of nickel-coated tungsten carbide powders by room temperature ultrasonic-assisted electroless plating. Surface and Coatings Technology, 2011, 206, 1091-1095.	4.8	48

#	Article	IF	CITATIONS
145	Longâ€Term Field Fertilization Significantly Alters Community Structure of Ammoniaâ€Oxidizing Bacteria rather than Archaea in a Paddy Soil. Soil Science Society of America Journal, 2011, 75, 1431-1439.	2.2	121
146	Optimization of Laccase-mediated Benzo[a]pyrene Oxidation and the Bioremedial Application in Aged Polycyclic Aromatic Hydrocarbons-contaminated Soil. Journal of Health Science, 2010, 56, 534-540.	0.9	20
147	Degradation of Polycyclic Aromatic Hydrocarbons by Crude Extracts from Spent Mushroom Substrate and its Possible Mechanisms. Current Microbiology, 2010, 60, 336-342.	2.2	69
148	Investigation of growth mechanism of nano-scaled cadmium sulfide within titanium dioxide nanotubes via solution deposition method. Applied Surface Science, 2010, 256, 6564-6568.	6.1	16
149	Heterogeneity of archaeal and bacterial ammoniaâ€oxidizing communities in Lake Taihu, China. Environmental Microbiology Reports, 2010, 2, 569-576.	2.4	77
150	Single-Crystalline Anatase TiO ₂ Dous Assembled Micro-Sphere and Their Photocatalytic Activity. Crystal Growth and Design, 2009, 9, 2324-2328.	3.0	61
151	Bioremediation of polycyclic aromatic hydrocarbons contaminated soil with Monilinia sp.: degradation and microbial community analysis. Biodegradation, 2008, 19, 247-257.	3.0	92
152	Fabrication of carbon-modified TiO2 nanotube arrays and their photocatalytic activity. Materials Letters, 2008, 62, 4579-4581.	2.6	46
153	Potential role of polycyclic aromatic hydrocarbons (PAHs) oxidation by fungal laccase in the remediation of an aged contaminated soil. Soil Biology and Biochemistry, 2008, 40, 789-796.	8.8	116
154	Pressureless infiltration of liquid aluminum alloy into SiC preforms to form near-net-shape SiC/Al composites. Journal of Alloys and Compounds, 2008, 465, 239-243.	5.5	62
155	Porous Copper Foamâ€based Plasmonic Nanocrystals Modified Threeâ€dimensional Semiconductor Nanoflowers for Multifold, Recyclable and Portable Detection of Environmental Contaminant. Particle and Particle Systems Characterization 0 2200072	2.3	1